

Complex Spatiotemporal Tuning in Human Upper-Limb Muscles

J. Andrew Pruszynski,^{1,*} Timothy P. Lillicrap,^{1,*} and Stephen H. Scott^{1,2,3}

¹Centre for Neuroscience Studies, ²Department of Anatomy and Cell Biology, and ³Department of Medicine, Queen's University, Kingston, Ontario, Canada

Submitted 25 August 2009; accepted in final form 15 November 2009

Pruszynski JA, Lillicrap TP, Scott SH. Complex spatiotemporal tuning in human upper-limb muscles. *J Neurophysiol* 103: 564–572, 2010. First published November 18, 2009; doi:10.1152/jn.00791.2009. Correlations between neural activity in primary motor cortex (M1) and arm kinematics have recently been shown to be temporally extensive and spatially complex. These results provide a sophisticated account of M1 processing and suggest that M1 neurons encode high-level movement trajectories, termed “pathlets.” However, interpreting pathlets is difficult because the mapping between M1 activity and arm kinematics is indirect: M1 activity can generate movement only via spinal circuitry and the substantial complexities of the musculoskeletal system. We hypothesized that filter-like complexities of the musculoskeletal system are sufficient to generate temporally extensive and spatially complex correlations between motor commands and arm kinematics. To test this hypothesis, we extended the computational and experimental method proposed for extracting pathlets from M1 activity to extract pathlets from muscle activity. Unlike M1 activity, it is clear that muscle activity does not encode arm kinematics. Accordingly, any spatiotemporal correlations in muscle pathlets can be attributed to musculoskeletal complexities rather than explicit higher-order representations. Our results demonstrate that extracting muscle pathlets is a robust and repeatable process. Pathlets extracted from the same muscle but different subjects or from the same muscle on different days were remarkably similar and roughly appropriate for that muscle's mechanical action. Critically, muscle pathlets included extensive spatiotemporal complexity, including kinematic features before and after the present muscle activity, similar to that reported for M1 neurons. These results suggest the possibility that M1 pathlets at least partly reflect the filter-like complexities of the periphery rather than high-level representations.

INTRODUCTION

Over a century of research has established that primary motor cortex (M1) plays a critical role in generating voluntary upper-limb movements, although considerable debate remains about the details of how M1 activity causes movement. To address this issue, many studies have examined how M1 activity is correlated to movement-related parameters at a fixed time delay. Indeed, correlations have been found with various parameters including hand direction (Georgopoulos et al. 1982; Schwartz et al. 1988), velocity (Moran and Schwartz 1999), force (Cheney and Fetz 1980; Evarts 1968; Hepp-Reymond et al. 1978; Sergio and Kalaska 1998), joint motion/torque (Gribble and Scott 2002; Herter et al. 2007; Scott and Kalaska 1997), and muscle activity (Morrow and Miller 2003). The observed correlations are sometimes taken as evidence that a

neuron's activity contributes to cause a given movement parameter at a fixed time delay.

An alternative link between M1 activity and movement, first proposed nearly 100 years ago (Leyton and Sherrington 1917), is that M1 neurons cause specific movement fragments. Indeed, electrical stimulation of M1 can result in complex, time-varying movements that appear to be part of a coordinated action (Brecht et al. 2004; Graziano et al. 2002). Recent work has highlighted this possibility by providing a sophisticated correlation technique and experimental paradigm to extract the movement fragments encoded by individual M1 neurons (Hatsopoulos et al. 2007). In that study, the authors trained monkeys to reach to randomly appearing spatial targets while recording activity from individual M1 neurons. The rich set of movements was then used to extract the kinematic trajectory (or “pathlet”) that was best correlated with the firing rate of individual M1 neurons. Strikingly, this extraction consistently resulted in pathlets that were spatially complex and temporally extensive. Extracted pathlets often spanned 400 ms and included dramatic changes in directional preference. More intriguingly, the discharge of a neuron correlated not only with future kinematic patterns, but also with kinematics that had already occurred.

Extracted pathlets provide a more sophisticated account of neural processing in M1. On the other hand, it is unclear whether extracted pathlets reveal a causal relationship between M1 activity and arm movement. Understanding the causal link is difficult because M1 activity can generate movement only via spinal processing (Perlmutter et al. 1998; Pierrot-Deseilligny and Burke 2005) and the substantial complexities of the musculoskeletal system, such as the force–velocity dependence of muscle (Joyce et al. 1969; Rack and Westbury 1969; Scott et al. 1996) and the inertial properties of the limb (Hogan 1985). These filter-like complexities can lead to correlations between M1 activity and time-invariant features of movement even if no such causal relationships are present (Mussa-Ivaldi 1988; Todorov 2000).

We hypothesized that M1 pathlets at least partly reflect complexities of the musculoskeletal system rather than high-level representations (Pruszynski et al. 2007). Although this is difficult to test directly, we can gain insight by extracting pathlets relating muscle activity and arm movement. It is clear that muscle activity does not encode high-level representations of arm movement; muscle activity causes muscular force that is then related to arm movement via Newtonian physics. Accordingly, if spatiotemporal features are present in muscle pathlets, they are likely the by-product of peripheral complexities, not high-level representations. Moreover, if muscle pathlets are similar to M1 pathlets, then M1 pathlets may also reflect peripheral complexities.

* These authors contributed equally to this work.

Address for reprint requests and other correspondence: S. H. Scott, Centre for Neuroscience Studies, Botterell Hall, Rm. 219, Queen's University, Kingston, ON, Canada K7L 3N6 (E-mail: steve@biomed.queensu.ca).

METHODS

Subjects

Seven university-aged subjects (five males; two females) participated in the experiment. One subject (#1) performed the same experiment on two separate days, for a total of eight analyzed experimental sessions. The first and second sessions from the same subject are referred to as “a” and “b,” respectively. All subjects were neurologically unimpaired, had normal or corrected-to-normal vision, and gave informed consent according to a protocol approved by the Queen’s University Research Ethics Board.

Apparatus

Subjects performed the experiments with a robotic exoskeleton (Kinesiological Instrument for Normal and Altered Reaching Movement [KINARM]; BKIN Technologies, Kingston, Ontario, Canada) that permits combined flexion and extension movements of the shoulder and elbow in the horizontal plane (Nozaki et al. 2006; Scott 1999). Target lights and simulated hand feedback were presented to the subject in the horizontal plane via a heads-up display composed of an overhead projector and semitransparent mirror.

Behavioral task

We used a modified version of the random-target pursuit task (Hatsopoulos et al. 2007). In brief, subjects reached to visual targets (radius = 1 cm) presented randomly within the arms’ workspace (24×24 -cm area centered on the hand when shoulder and elbow angles were 45° and 90° , respectively) (Fig. 1, *A* and *B*). When subjects reached the displayed target, it disappeared and another randomly

placed target appeared; this continued for 30 s per trial, with no constraints on how many targets could be reached in a trial. Subjects were instructed to reach at a comfortable pace and not encouraged to maximize the number of targets that they reached. A total of 60 such trials made up the experiment, which lasted about 90 min including setup time and breaks between trials.

Muscle activity

Surface electromyographic (EMG) recordings were obtained from up to seven upper-limb muscles involved with flexion or extension at the elbow and/or shoulder: brachioradialis (Br, monoarticular elbow flexor, $n = 7$), biceps long (Bi, biarticular flexor, $n = 8$), triceps lateral (TLat, monoarticular elbow extensor, $n = 8$), triceps long (TLo, biarticular extensor, $n = 8$), deltoid anterior (DA, monoarticular shoulder flexor, $n = 4$), deltoid posterior (DP, monoarticular shoulder extensor, $n = 8$), and pectoralis major (PM, monoarticular shoulder flexor, $n = 8$). Prior to electrode placement, the skin was cleaned and abraded with rubbing alcohol and the electrode contacts were covered with conductive gel. Electrodes (DE-2.1; Delsys, Boston, MA) were placed on the belly of the muscle oriented along the muscle fiber and the reference electrode (Dermatode; American Imex, Irvine, CA) was attached to the ankle. Signals were amplified (gain = 10^3 – 10^4) and band-pass filtered (20–450 Hz) by a commercially available system (Bagnoli; Delsys) then digitally sampled at 1,000 Hz. More details are provided in our previous publications (Pruszynski et al. 2008, 2009).

Encoding model

We used a modified version of the movement-fragment extraction technique originally introduced by Hatsopoulos and colleagues (2007)

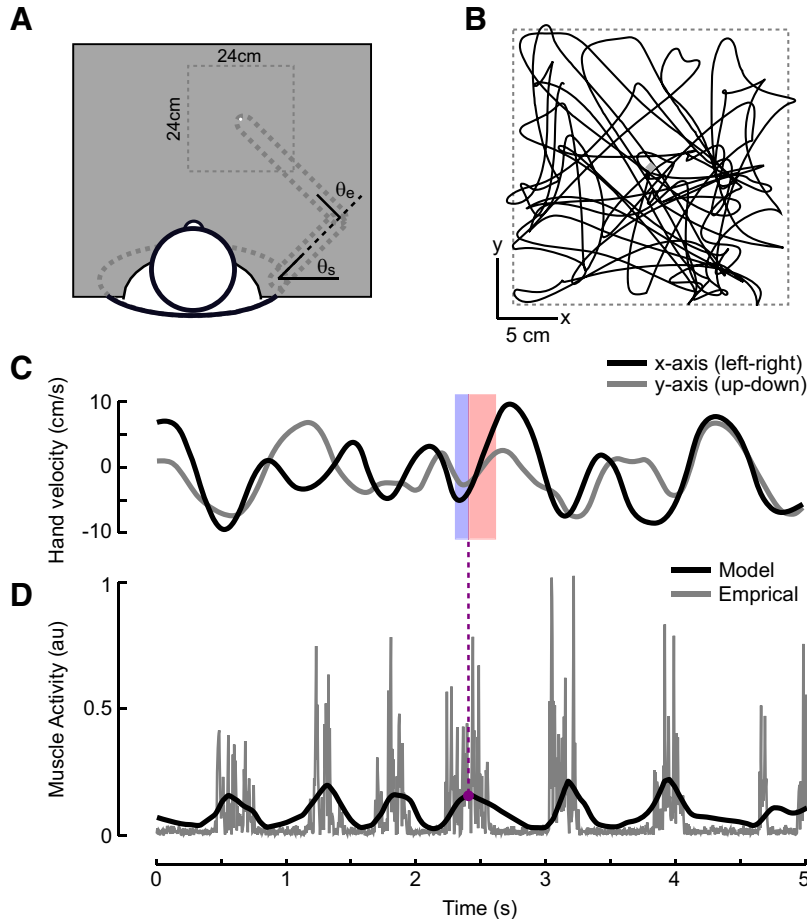


FIG. 1. Exemplar kinematics and muscle activity. *A*: subjects were presented with visual targets (radius = 1 cm) located randomly within a 24×24 cm area (dotted) centered at the tip of their index finger when shoulder (θ_s) and elbow angles (θ_e) were 45° and 90° , respectively. When subjects reached the currently displayed target, it would disappear and another target would be presented. Subjects were instructed to reach at a comfortable pace and not encouraged to maximize reached targets. *B*: exemplar hand trajectory for a single trial. The dotted gray line represents the extent of the target area. *C*: section of hand velocity (toward/away axis = gray line; left/right = black line) from a single trial. The red and blue filled areas show one section of hand velocity of optimal duration and offset (before/after time = $-100/+200$ ms) associated with a particular peak of muscle activity. *D*: empirical and model muscle activity from the same trial. The vertical axis represents the magnitude of muscle activity and is presented in arbitrary units. The gray line is muscle activity from a single muscle sample and the black line is the model prediction of muscle activity with the optimal pathlet duration and offset.

for neural data, in which a generalized linear model was used to determine the appropriate parameters for maximizing the likelihood of observing a neural spike (or not) within a small sampling window given a particular kinematic trajectory. In its simplest form this can be formalized as $P[\text{spike}(t) | \vec{v}^o] = \exp(k \cdot \vec{v}^o + \gamma)$, which is maximized when the kinematic trajectory (in terms of velocity, \vec{v}^o) is equal to that neuron's preferred velocity trajectory (k); γ is an offset parameter of the model.

We were interested in extracting preferred movement fragments for muscle activity as measured via electromyography (EMG). Since EMG signals are real-valued, we used a modified model that can be summarized as $P[\text{EMG}(t) | \vec{v}^o] \sim \text{Normal}[\exp(k \cdot \vec{v}^o + \gamma), \sigma^2]$, where $\text{EMG}(t)$ is the muscle activity, k is the muscle's preferred trajectory, \vec{v}^o is a particular (not normalized) velocity trajectory, and γ is an offset term. The sampling rate used for the modeling was 200 Hz. We maximized the probability of the data under this model by optimizing k and γ using the *fmincon* function in Matlab (The MathWorks, Natick, MA). That is, we minimized the sum of squared error between predicted and actual EMG for each muscle sample. Integrated versions of these velocity trajectories are used for visual representations of the empirical data and thus represent preferred spatial paths, or "pathlets."

The optimal pathlet duration and shift were calculated across all our collected muscle samples by ranking the ability of 80 potential pathlets (ranging from 50 to 500 ms in duration and -100 to 250 in shift) to predict EMG activity on a test set (last 30 of the 60 collected trials) of kinematic/EMG data not used for fitting the model. Specifically, we ranked each pathlet for every individual muscle sample according to the sum of squared error between its prediction of EMG and the actual EMG on the test set. The optimal pathlet was then defined as that which, on average, yielded the best rank across muscle samples.

Testing the encoding model

To confirm the functionality of the extraction technique we created a data set of synthetic muscle activity. We used the encoding model to generate EMG output [$\text{EMG}(t)$] given a particular preferred velocity trajectory (the "true" trajectory, k) and a set of hand velocities taken from empirical data generated by Subject 1b; the offset parameter (γ) was set to 0.

We chose a true preferred velocity trajectory that was spiral-shaped, had a duration (temporal length of trajectory around *time 0*) of 300 ms, and a shift (temporal offset of trajectory center) of $+50$ ms (Fig. 2A). Such a trajectory incorporates kinematic data from -100 ms before the current EMG to $+200$ ms afterward and thus we sometimes refer to these trajectories with respect to their temporal extent before/after the current EMG [$-100/+200$ ms, equivalent to lead/lag notation used in Hatsopoulos et al. (2007)]. It is important to clarify the mapping between the duration/shift parameters and before/after notation. The duration parameter refers to the overall length of the pathlet that, by default, is centered at 0 ms. A pathlet with 300-ms duration and 0-ms shift incorporates kinematic data from -150 ms before to $+150$ ms after the current EMG. The shift term then determines the placement of the center of the pathlet. Thus a pathlet with 300-ms duration and $+100$ -ms shift would incorporate kinematic data from -50 ms before to $+250$ ms after the current EMG.

Given the synthetic EMG and a subset of the same kinematic data set (first 30 trials from Subject 1b), we attempted to extract the preferred velocity trajectory using the encoding model described earlier. That is, we estimated k and γ from the model for 80 potential preferred velocity shifts/durations (duration: ranging from 50 to 500 ms in 50-ms intervals, 10 durations total; shift: ranging from -100 to $+250$ ms in 50-ms intervals, 8 shifts total). We then ranked the 80 candidate preferred trajectories by their ability to predict the synthetic EMG as measured by the sum of squared error between predicted and synthetic EMG. Note that we compared EMG from only the second half of the kinematic data set that was not used to extract the preferred velocity trajectories. If the extraction technique is working well, the best-ranked preferred velocity trajectories should have spatiotemporal properties similar to those of the true preferred velocity trajectory. Ideally, our technique would choose the preferred velocity trajectory with a spiral-like shape and duration and shift of 300 and $+50$ ms, respectively (before/after = $-100/+200$ ms).

RESULTS

Features of behavior

Subjects had little difficulty learning the task and were able to move smoothly and accurately between targets. On average,

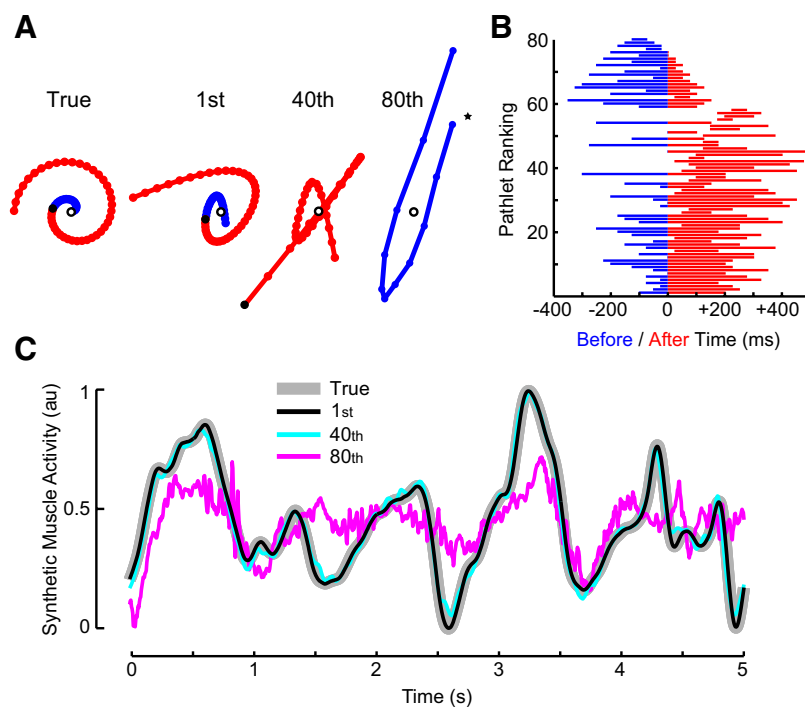


FIG. 2. Testing the encoding model. *A*: the "true" preferred velocity trajectory used to generate synthetic muscle activity for testing pathlet extraction (duration: 300 ms; offset: $+50$ ms). The next 3 trajectories are those extracted from the synthetic muscle activity (see METHODS). Dots are placed on each trajectory at 5-ms intervals. Numbers indicate trajectory rank (1st = best) in predicting the synthetic muscle activity on a test set of kinematic data among 80 candidates. For each trajectory, blue and red portions represent time before and after current muscle activity, respectively; before/after are referred to as lead/lag time in Hatsopoulos et al. (2007). The white dot represents the origin and all trajectories are on the same arbitrary scale. The black dot represents *time 0* relative to muscle activity. For the 80th ranked trajectory, which incorporates time only before current muscle activity, the star indicates the beginning of the trajectory. *B*: ranking of all candidate trajectories. The horizontal axis represents time before (blue) and after (red) current muscle activity. The vertical axis represents trajectory ranking for predicting muscle activity on a data set not used to fit the model. Each line represents one of the 80 tested trajectories. *C*: synthetic and extracted muscle activity from a small portion of one test-set trial. The vertical axis represents the magnitude of muscle activity in arbitrary units. The gray line is the synthetic muscle activity generated by the true trajectory shown in *A*. The black, cyan, and purple are predictions of muscle activity by the 1st, 40th, and 80th ranked trajectories, respectively.

subjects reached 41 targets (SD = 12) per trial, although there were significant differences between subjects [range = 23–52 targets; two-way ANOVA, subjects \times trial number, main effect of subject, $F_{(6,209)} = 303$, $P < 10^{-6}$]. Such differences are not surprising, given that subjects were instructed to reach at a comfortable pace and were not encouraged to maximize the number of targets. Notably, there was no significant increase or decrease in the number of targets per trial [main effect of trial number, $F_{(29,209)} = 0.7$, $P = 0.84$], suggesting that the task did not induce substantial learning or fatigue and that subjects maintained a similar strategy throughout the experimental session. Robust behavioral stability was found in one subject who completed the same experiment on two separate days and showed a modest, though significant, decrease in the number of targets achieved per trial in the second experimental session [day 1: 52 targets per trial (SD 8); day 2: 50 targets per trial (SD 4); t -test, $t_{118} = 2.2$, $P = 0.03$].

Functionality of the extraction technique

We confirmed the functionality of the extraction technique by creating a synthetic data set of muscle activity using a known preferred velocity trajectory (duration: 300 ms; shift: 50 ms; spiral-like shape; Fig. 2A, “true”) coupled with empirical hand-velocity kinematics (see METHODS). The preferred trajectory best able to predict the synthetic muscle activity (lowest sum of squared error on the test data set) from 80 candidates had spatiotemporal features (duration/shift: 300/–100 ms; spiral-like shape; Fig. 2A, labeled “1st”) that were very similar to those of the true trajectory and such similarity clearly decreased for worse-ranked trajectories (Fig. 2A, labeled “40th” and “80th”). Furthermore, there was clear structure in the ranking whereby better trajectories tended to have a duration and shift similar to those of the true trajectory (Fig. 2B). Although the spatiotemporal differences among candidate trajectories were substantial, even the worst-ranked trajectory captured the basic features of the synthetic muscle activity (Fig. 2C). We found no substantial difference between the synthetic and predicted muscle activity for the best-ranked trajectory (correlation coefficient, $r = 0.999$) and even the 40th ranked trajectory generated good predictions ($r = 0.993$). The correlation for the worst-ranked trajectory was substantially lower ($r = 0.581$).

Extracting pathlets from muscle activity

Muscle activity was collected via electromyography (EMG) from up to seven muscles from each subject. Each arm muscle sample showed clear phasic activity associated with reaching in both agonist and antagonist phases of movement (Fig. 1, C and D).

The principal interests of the present study were 1) to extract pathlets from simultaneously collected muscle activity and kinematic data and 2) to determine the extent to which muscle pathlets demonstrated spatiotemporal complexity. We first ranked each of the 80 pathlets (ranging from 50 to 500 ms in duration and –100 to 250 in shift) in order of their ability to predict the actual EMG on a test set of data not used to fit the pathlets (i.e., the sum of squared error; see Fig. 3A for an exemplar ranking and Fig. 1D for an exemplar EMG prediction). We then found the optimal pathlet duration and shift by

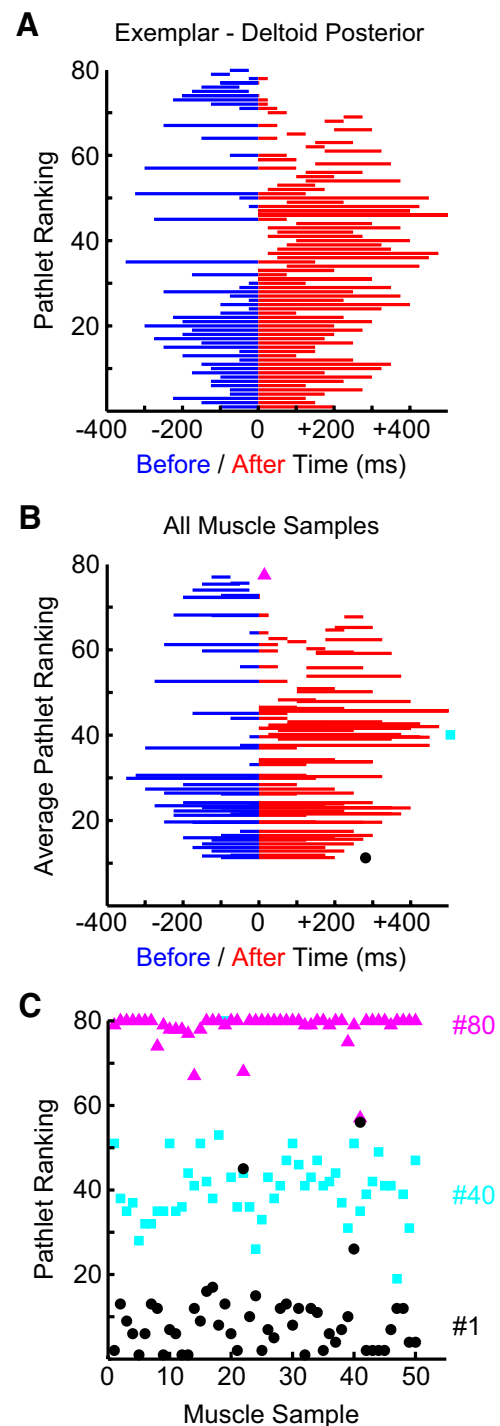


FIG. 3. Pathlet selection and ranking. *A*: ranking of pathlets for an exemplar muscle (deltoid posterior, Subject 1a), same format as that in Fig. 2B. *B*: same format as that in *A* except that the vertical axis represents mean ranking across samples. The 3 symbols mark the pathlets shown in *C*. *C*: ranking of 3 exemplar pathlets (black, optimal pathlet, ranked 1st; cyan, 40th; purple, 80th) for each collected muscle sample. The horizontal and vertical axes represent muscle sample and pathlet rank, respectively.

ranking the ability of the 80 potential pathlets in terms of their average rank across all muscle samples (Fig. 3B). The optimal pathlet was 300 ms in duration and had a +50-ms offset and thus incorporated kinematics ranging from –100 ms before to +200 ms after the current EMG activity (before/after referred

to as lead/lag in Hatsopoulos et al. 2007). Across all muscle samples, this optimal pathlet had a mean rank of 10th (SD 13; median rank = 7th) and was ranked in the top 10% of pathlets in 60% of all samples (Fig. 3B). On average, the predictions made by the optimal pathlet had a correlation of 0.277 (SD 0.123) with EMG from the test set, compared with correlations of 0.097 (SD 0.065) and 0.280 (SD 0.127) for the worst- and best-ranked pathlets on each sample, respectively.

As with M1 neurons (Hatsopoulos et al. 2007), there was a clear trend whereby the best pathlets tended to be long in duration and incorporated kinematic information both before and after current muscle activity. In fact, the average length of optimal pathlets determined for each muscle sample was 297 ms (SD 84) and nearly all muscle samples (49/50, 98%) yielded optimal pathlets that included time both before and after the current muscle activity.

Pathlet rankings were impressively stable across muscle samples, with no significant difference in optimal pathlet duration as a function of muscle [two-way ANOVA; $F_{(6,49)} = 0.86$, $P = 0.53$] or subject [$F_{(6,49)} = 0.83$, $P = 0.57$]. Such stability is demonstrated in Fig. 3C, which shows the ranking of three exemplar pathlets (that ranked 1st, 40th, and 80th across the population) for every collected muscle sample; note the stability in the pathlet ranking, with the best pathlet consistently performing well and the worst pathlet performing almost universally poorly.

After selecting the optimal pathlet duration and shift, we calculated the pathlet for each collected muscle sample using the optimal duration/shift. The resultant pathlet shapes can be broadly understood with respect to the mechanical action of the muscle from which they were extracted. For example, deltoid posterior, a muscle that generates shoulder extensor torque, resulted in pathlets that included slowing of movements to the left and slightly away from the body followed by dramatic increases in velocity directed to the right and slightly toward the body (Fig. 4, A–C). The involvement of deltoid posterior in rightward velocities can be understood from the muscles' mechanical action since generation of shoulder extension velocity results mostly in rightward hand velocity throughout the workspace of the task. This is shown in Fig. 4D, where we plot the hand velocity that results from a unit shoulder extension velocity at various locations in the workspace. Another principal feature of the trajectory—the presence of a countermovement—where rightward movements are preceded by leftward ones (approximately –50 to 100 ms on Fig. 4A), likely reflects the muscle activity required to slow the inertial mass of the arm as it is moving leftward and reaccelerate it to the right.

The extracted pathlets for other muscles could be similarly understood by their mechanics and the task constraints (Fig. 5). Pectoralis major, a shoulder flexor largely involved in the generation of shoulder flexion velocity (Figs. 4G and 5, PM) resulted in pathlets that were essentially opposite to those for deltoid posterior (Figs. 4, D–F and 5, DP). Pathlets from

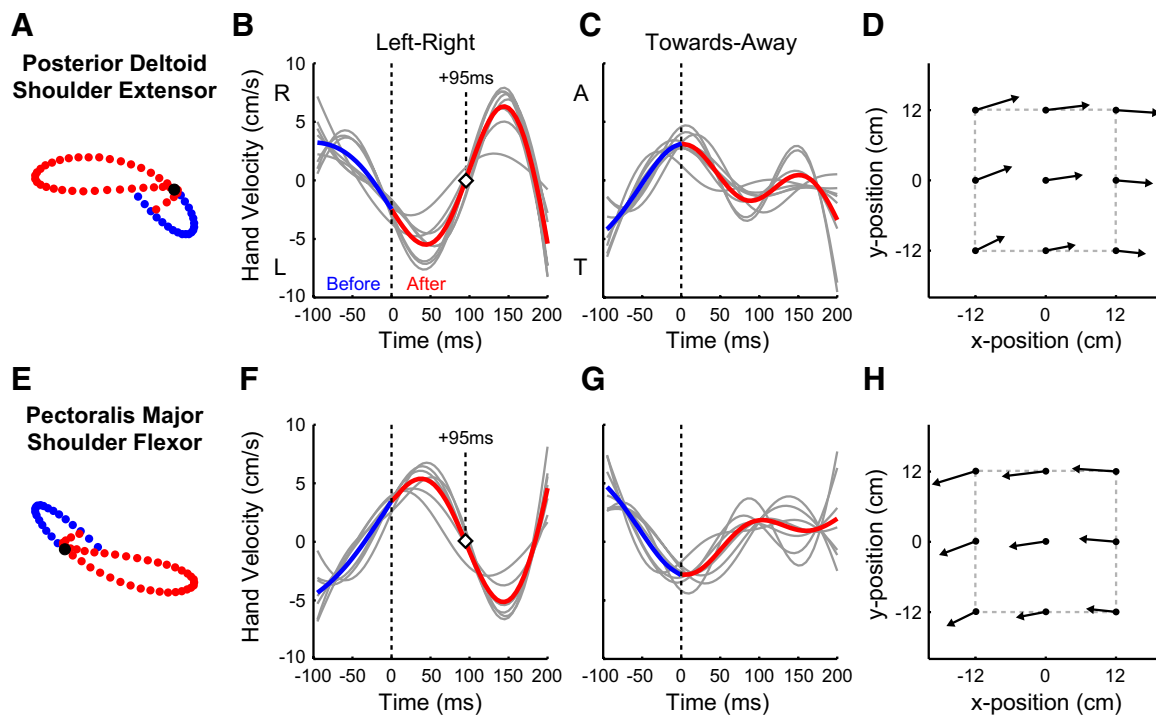


FIG. 4. Preferred velocity trajectory with respect to time. A: mean extracted pathlet using the optimal duration and shift (–100 ms before to +200 ms after the current electromyogram [EMG]) for deltoid posterior, a shoulder extensor. Format for pathlets is the same as that in Fig. 2A. B: preferred velocity trajectory along the left–right axis (left = negative velocity; right = positive) in external space for deltoid posterior. Each thin gray line is a trajectory generated from an individual subject and the thick line represents the mean trajectory. Negative and positive times on the horizontal axis are before and after the current muscle activity (blue and red, respectively, for the mean trajectory). The vertical axis represents hand velocity. The white diamond (at +95 ms) represents the time of peak acceleration. C: same format as that in B except for movement toward and away (toward = negative velocity; away = positive) from the body. Note that the integral of this preferred velocity trajectory in both dimensions (B and C) is a pathlet as shown in A. D: direction and relative magnitude of hand velocity caused by the same shoulder extension velocity at different locations in the workspace. The base of each vector represents the hand position at which the shoulder velocity is generated. Note the similarity of the resultant hand velocity for all locations in the workspace. E–G: same format as that in A–D except for pectoralis major, a shoulder flexor.

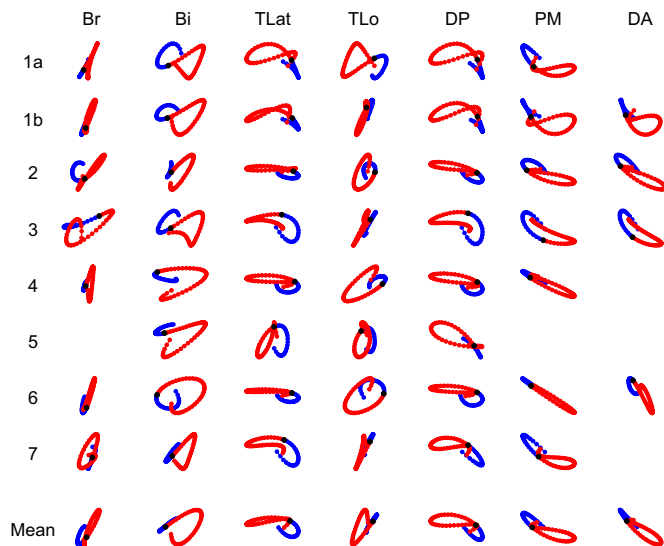


FIG. 5. Extracted pathlets from each muscle sample. Each panel represents the extracted pathlet using the optimal duration and shift (-100 ms before to $+200$ ms after the current EMG) as described in Fig. 2A. The columns and rows represent muscle and subjects, respectively. Subject 1a and 1b refer to data sets from the same subject but different sessions. The last row represents the mean pathlet for each muscle. Depicted pathlets represent integrated version of the optimal velocity trajectory and thus can be thought to represent a spatial path, or pathlet. Empty cells reflect the fact that we did not collect muscle activity for all candidate muscles from every subject.

deltoid anterior, a synergistic shoulder flexor, demonstrate patterns similar to those of pectoralis major (Fig. 5, DA). Elbow muscle pathlets were oriented away from the body and to the right for extensors (Fig. 5, TLat) and toward the body and to the left for flexors (Fig. 5, Br), which again closely mirrors their mechanical action at the elbow for the given arm orientation and the workspace of the task. Last, pathlets from biarticular muscles (Fig. 5, Bi and TLo) appear qualitatively intermediate to monoarticular shoulder flexor and elbow flexor muscle pathlets.

These pathlets indicate that there is a complex relationship between EMG activity and hand motion, whereby pathlets often change direction within the temporal extent of their duration. Given their complex shape, pathlets were impressively robust with a striking similarity in shape for the same muscle across subjects (columns in Fig. 5), with a mean pairwise correlation (r) between pathlets of 0.72 (SD 0.23). Such correlations were moderate to high for all collected arm muscles: biceps (0.70, SD 0.18), brachioradialis (0.49, SD 0.37), triceps lateral (0.72, SD 0.22), triceps long (0.69, SD 0.20), pectoralis major (0.83, SD 0.09), deltoid anterior (0.65, SD 0.19), and deltoid posterior (0.85, SD 0.09). When comparing correlations across muscles groups, we found a systematic pattern for different muscle group combinations (Table 1). Muscle samples from the same muscle group were highly correlated, muscles with similar mechanical actions (i.e., synergists) were positively correlated, muscles with opposite mechanical action were negatively correlated, and muscles that spanned different joints demonstrated weak and/or inconsistent correlations. Last, we found that pathlets were particularly consistent between muscle samples for the same subject collected in two different sessions (labeled 1a and 1b on Fig. 5), with a mean correlation coefficient of 0.94 (SD 0.07).

TABLE 1. Correlation coefficients (r) of hand-based pathlets across subjects

	Br	Bi	TLat	TLo	PM	DA	DP
Br	0.49						
Bi	0.50	0.70					
TLat	-0.17	-0.53	0.72				
TLo	-0.59	-0.67	0.30	0.69			
PM	-0.02	0.37	-0.75	-0.08	0.83		
DA	-0.18	0.19	-0.59	0.10	0.76	0.65	
DP	-0.02	-0.44	0.78	0.15	-0.85	-0.71	0.85

We applied the same encoding model in a joint-velocity coordinate system to quantify the preferred trajectory of upper-limb muscles relative to shoulder and elbow joint movements. As with hand-based pathlets, we found that better joint-based pathlets (in terms of predicting EMG on the test set) tended to be temporally extensive and incorporate movements both before and after the current EMG (Fig. 6A). The optimal pathlet chosen was 150 ms in duration with a 0-ms shift [mean rank of 7th (SD 13); median rank = 4th, in top 10%: 82% of samples] and thus included kinematics from -75 ms before to $+75$ ms after the current EMG, substantially shorter than the optimal hand-based pathlet that was 300 ms in duration. In fact, across all collected muscle samples, the best-ranked pathlets in joint-space were significantly shorter than those extracted in hand-space [joint: 104 ms (SD 87); hand: 297 ms (SD 84); t -test, $t_{98} = -11.3$; $P < 10^{-3}$]. There was no significant difference in optimal pathlet duration as a function of muscle [two-way ANOVA; $F_{(6,49)} = 0.36$, $P = 0.90$] or subject [$F_{(6,49)} = 1.07$, $P = 0.39$].

Joint-based pathlets were very robust, with a mean pairwise correlation across multiple samples of the same muscle of 0.80 (SD 0.15) and a systematic pattern of correlations for different muscle group combinations as seen for hand-based pathlets (Table 2). As with hand-based pathlets, joint-based pathlets could be understood by the mechanical action of the muscle from which it was extracted (Fig. 6B). For example, deltoid posterior, a muscle that generated shoulder extensor torque resulted in pathlets that included slowing of shoulder flexor movements midway through the pathlet, followed by increases in velocity in the shoulder extensor direction (see last few red data points in Fig. 6B). The opposite pattern was observed for

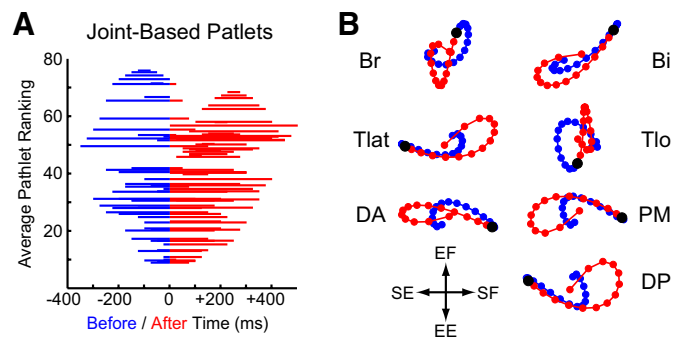


FIG. 6. Pathlet extraction in joint coordinates. A: average ranking of pathlets across subjects and muscles. Same format as that in Fig. 3B. B: mean pathlets for each muscle sample. Format is the same as that in Fig. 5, except that the axes are presented in joint-space where left, right, down, and up represent shoulder extension, shoulder flexion, elbow extension, and elbow flexion, respectively.

TABLE 2. Correlation coefficients (r) of joint-based pathlets across subjects

	Br	Bi	TLat	TLo	PM	DA	DP
Br	0.68						
Bi	0.70	0.85					
TLat	-0.17	-0.58	0.73				
TLo	-0.79	-0.56	-0.03	0.93			
PM	-0.09	0.55	-0.82	-0.17	0.90		
DA	-0.20	0.60	-0.76	0.02	0.85	0.78	
DP	-0.007	-0.48	0.81	-0.27	-0.91	-0.82	0.92

deltoid anterior and pectoralis major, consistent with their mechanical action as generators of shoulder flexion.

DISCUSSION

In the present experiment, we investigated whether correlations between muscle activity and arm kinematics (i.e., pathlets) were temporally extensive and spatially complex. We used a modified version of the computational and experimental approach applied previously for determining spatiotemporal correlations between M1 neurons and arm kinematics (Hatsopoulos et al. 2007). Subjects reached to randomly appearing targets while we recorded arm kinematics and muscle activity from multiple muscles spanning the shoulder and elbow, including mono- and biarticulars. Unlike standard center-out reaching tasks (Georgopoulos et al. 1982), where subjects make stereotyped movements between a central target and a small number of peripheral targets, random-target pursuit results in an extensive set of reaching profiles sampling a wide range of positions and velocities in the arm's workspace. The extensive sampling of arm kinematics allowed us to construct a general linear model to find the spatiotemporal hand-velocity (and joint-velocity) trajectory, which maximized our ability to predict muscle activity. Integrated versions of optimal velocity trajectories represent optimal spatial paths and are termed "pathlets."

An impressive feature of the present results is the reproducibility of the pathlet extraction process. We first tested our ability to extract pathlets by creating a synthetic data set of muscle activations based on known pathlet and kinematic profiles taken from the empirical data. We successfully recovered the underlying pathlet (Fig. 2), suggesting that the technique, and our implementation of it, worked well. When pathlets were extracted for the same muscle across subjects, the resulting pathlets were very similar (Figs. 5 and 6) and the correlation between pathlets was impressive (Tables 1 and 2). When the same subject repeated the experiment in two different experimental sessions, the extracted pathlets were extremely similar (compare Subject 1a with 1b in Fig. 4). Taken together, these results suggest that extracting spatiotemporal trajectories is a reliable and effective method of describing the relationship between arm kinematics and muscle activity.

Our results demonstrate that muscle pathlets are temporally extensive and spatially complex. Optimal muscle pathlets in hand-based coordinates included movements from 100 ms before to 200 ms after the current EMG; optimal pathlets in joint coordinates were substantially shorter, although the optimal pathlet still incorporated movements from 75 ms before to 75 ms after the current EMG. In both coordinate systems, there was a clear trend favoring pathlets that included time both

before and after the current EMG (Figs. 3B and 6A). Extracted pathlets were also spatially complex, often changing direction midway through their span, although such changes could be readily understood from the mechanical action of a given muscle. For example, the optimal hand-based pathlet for posterior deltoid, a muscle that extends the shoulder, starts moving toward the left and away from the body (before the current EMG), and then shows an abrupt change in direction and ends moving to the right and toward the body (after the current EMG), which is broadly consistent with the generation of shoulder extension torque (the expected contribution of this muscle) to decelerate the shoulder and then accelerate it in the opposite direction. A similar interpretation can be made with the joint-based pathlet for deltoid posterior (Fig. 6B).

Since muscles have no high-level representations of arm kinematics, muscle pathlets are likely the by-product of the complexities of transforming muscle activity into muscle force (Brown and Loeb 1999, 2000a,b; Brown et al. 1999; Zajac 1989) and the Newtonian relationship between muscle forces and arm kinematics. For example, muscles change their effectiveness at generating force as a function of muscle length (Rack and Westbury 1969) and velocity (Joyce et al. 1969; Scott et al. 1996) and the conversion from muscle forces to arm kinematics is sensitive to the geometry of the limb and its inertial properties (Hogan 1985). Furthermore, the temporal relationship between muscle activity and muscle force and eventual arm kinematics is not instantaneous. Muscle activity leads to muscle force only after a substantial delay, with an activation time constant of about 50 ms, and the muscle continues to generate force when muscle activity has ceased, with a deactivation time constant of about 65 ms (Bawa and Stein 1976; Brown and Loeb 2000b). Even after muscle force is generated it must integrate over time to cause changes in hand acceleration, velocity, and position (resulting in autocorrelations in the kinematic signals). It is these complex-state dependencies, temporal delays, and autocorrelations that preclude a simple mapping between muscle activity and arm kinematics, resulting in pathlets that are spatially complex and temporally extensive when viewed relative to hand- or joint-based coordinates.

Although extracted pathlets were complex in both hand and joint coordinates, we found that joint-based pathlets were significantly shorter in duration than hand-based pathlets. This reduced duration likely reflects the fact that a muscle's force is more closely related to the generation of velocity at its spanned joint(s) rather than the generation of velocity in hand-based coordinates. Consider the action of a monoarticular elbow flexor muscle at two different arm configurations: 1) shoulder angle of 0° and elbow angle of 90°; 2) shoulder angle of 90° and elbow angle of 90° (angles as defined in Fig. 1A). With respect to joint coordinates, the action of the elbow flexor would result in consistent elbow flexion movements for both configurations (this mapping is not perfect because of the inertial properties of the limb). In contrast, there is a dramatic change in the mapping between muscle action and hand coordinates across arm configuration. The same elbow flexion muscle force would yield largely leftward movements in the first configuration and largely downward movements in the second configuration. A similar, though less dramatic, rotation would be present for shoulder muscles and can be seen in Fig. 4, D and G. It is important to stress that although muscle forces are statistically related to joint motion (Graham et al. 2003), this relationship is not direct. For example, muscle force at the

shoulder will result in motion of both the shoulder and elbow due to the mechanical interactions between limb segments (Hollerbach and Flash 1982).

The present results cannot explicitly rule out the possibility that M1 neurons do encode high-level movement trajectories; however, they do demonstrate that pathlets based on arm kinematics would look similar, irrespective of whether M1 neurons encoded high-level movement trajectories or low-level muscle activity. In short, our results caution against interpreting correlations between M1 activity and high-level movement features as indicative of the causal relationship between M1 and movement (Churchland and Shenoy 2007; Fetz 1992; Mussa-Ivaldi 1988; Robinson 1992; Todorov 2000).

Although pathlets may not reveal causal links between motor commands and arm kinematics, they do provide a more sophisticated account of motor commands and their relationship to arm movement than time-invariant representations. For example, pathlets provide a natural description of changing preferred directions that have been observed in several studies of M1 (Mason et al. 1998; Sergio and Kalaska 1998). They could also account for the known idiosyncratic sensitivity of M1 directional tuning to reach velocity, distance, and time (Churchland and Shenoy 2007). Furthermore, the observation that M1 activity is related to kinematics that have already occurred is consistent with the robust presence of peripheral feedback in M1 (Conrad et al. 1975; Evarts 1968; Herter et al. 2009), a well-established result that is overlooked by many recent studies focusing on time-invariant representations. Most important, perhaps, decoding hand trajectories from a population of M1 neurons is improved when assuming pathlet representations (Hatsopoulos et al. 2007), a result that will likely lead to improved performance of neural prosthetics and brain-machine interfaces.

ACKNOWLEDGMENTS

We thank K. Moore for technical and logistical support and the members of the Scott Lab, especially A. Coderre and I. Kurtzer, for fruitful discussions leading to this manuscript.

GRANTS

This work was supported by the National Science and Engineering Research Council of Canada, Canadian Institutes of Health Research salary awards to J. A. Pruszynski and S. H. Scott, and a Ontario Graduate Scholarship Program salary award and Sun Microsystems of Canada Scholarship in Computational Sciences and Engineering to T. P. Lillicrap. Some simulations were carried out using resources provided by the High Performance Computing Virtual Laboratory.

DISCLOSURES

S. H. Scott is associated with BKIN Technologies, which commercializes the KINARM robot.

REFERENCES

- Bawa P, Stein RB. Frequency-response of human soleus muscle. *J Neurophysiol* 39: 788–793, 1976.
- Brecht M, Schneider M, Sakmann B, Margrie TW. Whisker movements evoked by stimulation of single pyramidal cells in rat motor cortex. *Nature* 427: 704–710, 2004.
- Brown IE, Cheng EJ, Loeb GE. Measured and modeled properties of mammalian skeletal muscle. II. The effects of stimulus frequency on force–length and force–velocity relationships. *J Muscle Res Cell Motil* 20: 627–643, 1999.
- Brown IE, Loeb GE. Measured and modeled properties of mammalian skeletal muscle. I. The effects of post-activation potentiation on the time course and velocity dependencies of force production. *J Muscle Res Cell Motil* 20: 443–456, 1999.
- Brown IE, Loeb GE. Measured and modeled properties of mammalian skeletal muscle. III. The effects of stimulus frequency on stretch-induced force enhancement and shortening-induced force depression. *J Muscle Res Cell Motil* 21: 21–31, 2000a.
- Brown IE, Loeb GE. Measured and modeled properties of mammalian skeletal muscle. IV. Dynamics of activation and deactivation. *J Muscle Res Cell Motil* 21: 33–47, 2000b.
- Cheney PD, Fetz EE. Functional classes of primate corticomotoneuronal cells and their relation to active force. *J Neurophysiol* 44: 773–791, 1980.
- Churchland MM, Shenoy KV. Temporal complexity and heterogeneity of single-neuron activity in premotor and motor cortex. *J Neurophysiol* 97: 4235–4257, 2007.
- Conrad B, Meyerlohmann J, Matsunami K, Brooks VB. Precentral unit-activity following torque pulse injections into elbow movements. *Brain Res* 94: 219–236, 1975.
- Evarts EV. Relation of pyramidal tract activity to force exerted during voluntary movement. *J Neurophysiol* 31: 14–27, 1968.
- Fetz EE. Are movement parameters recognizably coded in the activity of single neurons? *Behav Brain Sci* 15: 679–690, 1992.
- Georgopoulos AP, Kalaska JF, Caminiti R, Massey JT. On the relations between the direction of two-dimensional arm movements and cell discharge in primate motor cortex. *J Neurosci* 2: 1527–1537, 1982.
- Graham KM, Moore KD, Cabel DW, Gribble PL, Cisek P, Scott SH. Kinematics and kinetics of multijoint reaching in nonhuman primates. *J Neurophysiol* 89: 2667–2677, 2003.
- Graziano MSA, Taylor CSR, Moore T. Complex movements evoked by microstimulation of precentral cortex. *Neuron* 34: 841–851, 2002.
- Gribble PL, Scott SH. Overlap of internal models in motor cortex for mechanical loads during reaching. *Nature* 417: 938–941, 2002.
- Hatsopoulos NG, Xu QQ, Amit Y. Encoding of movement fragments in the motor cortex. *J Neurosci* 27: 5105–5114, 2007.
- Hepp-Reymond MC, Wyss UR, Anner R. Neuronal coding of static force in the primate motor cortex. *J Physiol (Paris)* 74: 287–291, 1978.
- Herter TM, Korbel T, Scott SH. Comparison of neural responses in primary motor cortex to transient and continuous loads during posture. *J Neurophysiol* 101: 150–163, 2009.
- Herter TM, Kurtzer I, Cabel DW, Haunts KA, Scott SH. Characterization of torque-related activity in primary motor cortex during a multijoint postural task. *J Neurophysiol* 97: 2887–2899, 2007.
- Hogan N. The mechanics of multi-joint posture and movement control. *Biol Cybern* 52: 315–331, 1985.
- Hollerbach JM, Flash T. Dynamic interactions between limb segments during planar arm movement. *Biol Cybern* 44: 67–77, 1982.
- Joyce GC, Rack PMH, Westbury DR. Mechanical properties of cat soleus muscle during controlled lengthening and shortening movements. *J Physiol* 204: 461–476, 1969.
- Leyton SS, Sherrington CS. Observations on the excitable cortex of the chimpanzee, orangutan and gorilla. *Q J Exp Physiol* 11: 135–222, 1917.
- Mason CR, Johnson MTV, Fu QG, Gomez JE, Ebner TJ. Temporal profile of the directional tuning of the discharge of dorsal premotor cortical cells. *Neuroreport* 9: 989–995, 1998.
- Moran DW, Schwartz AB. Motor cortical representation of speed and direction during reaching. *J Neurophysiol* 82: 2676–2692, 1999.
- Morrow MM, Miller LE. Prediction of muscle activity by populations of sequentially recorded primary motor cortex neurons. *J Neurophysiol* 89: 2279–2288, 2003.
- Mussa-Ivaldi FA. Do neurons in the motor cortex encode movement direction? An alternative hypothesis. *Neurosci Lett* 91: 106–111, 1988.
- Nozaki D, Kurtzer I, Scott SH. Limited transfer of learning between unimanual and bimanual skills within the same limb. *Nat Neurosci* 9: 1364–1366, 2006.
- Perlmutter SI, Maier MA, Fetz EE. Activity of spinal interneurons and their effects on forearm muscles during voluntary wrist movements in the monkey. *J Neurophysiol* 80: 2475–2494, 1998.
- Pierrot-Deseilligny E, Burke D. *The Circuitry of the Spinal Cord: Its Role in Motor Control and Movement Disorders*. Cambridge, UK: Cambridge Univ. Press, 2005.
- Pruszynski JA, Coderre AM, Lillicrap TP, Kurtzer I. Temporal encoding of movement in motor cortical neurons. *J Neurosci* 27: 10076–10077, 2007.
- Pruszynski JA, Kurtzer I, Lillicrap TP, Scott SH. Temporal evolution of “automatic gain-scaling.” *J Neurophysiol* 102: 992–1003, 2009.

- Pruszynski JA, Kurtzer I, Scott SH.** Rapid motor responses are appropriately tuned to the metrics of a visuospatial task. *J Neurophysiol* 100: 224–238, 2008.
- Rack PMH, Westbury DR.** Effects of length and stimulus rate on tension in isometric cat soleus muscle. *J Physiol* 204: 443–460, 1969.
- Robinson DA.** Implications of neural networks for how we think about brain function. *Behav Brain Sci* 15: 644–655, 1992.
- Schwartz AB, Kettner RE, Georgopoulos AP.** Primate motor cortex and free arm movements to visual targets in 3-dimensional space. 1. Relations between single cell discharge and direction of movement. *J Neurosci* 8: 2913–2927, 1988.
- Scott SH.** Apparatus for measuring and perturbing shoulder and elbow joint positions and torques during reaching. *J Neurosci Methods* 89: 119–127, 1999.
- Scott SH, Brown IE, Loeb GE.** Mechanics of feline soleus. 1. Effect of fascicle length and velocity on force output. *J Muscle Res Cell Motil* 17: 207–219, 1996.
- Scott SH, Kalaska JF.** Reaching movements with similar hand paths but different arm orientations. I. Activity of individual cells in motor cortex. *J Neurophysiol* 77: 826–852, 1997.
- Sergio LE, Kalaska JF.** Changes in the temporal pattern of primary motor cortex activity in a directional isometric force versus limb movement task. *J Neurophysiol* 80: 1577–1583, 1998.
- Todorov E.** Direct cortical control of muscle activation in voluntary arm movements: a model. *Nat Neurosci* 3: 391–398, 2000.
- Zajac FE.** Muscle and tendon: properties, models, scaling, and application to biomechanics and motor control. *Crit Rev Biomed Eng* 17: 359–411, 1989.